Study on the surface formation mechanism in scratching test with different ultrasonic vibration forms

Zhen Li [a,b], Songmei Yuan [c,*], Jiang Ma [a,*], Jun Shen [a], Andre D.L. Batako [d]

[a] College of Mechatronics and Control Engineering, Shenzhen University, Shenzhen, 518060, China
[b] College of Physics and Optoelectronic Engineering, Shenzhen University, Shenzhen, 518060, China
[c] School of Mechanical Engineering and Automation, Beihang University, Beijing, 100191, China
[d] General Engineering Research Institute, Liverpool John Moores University, Liverpool, L3 5UX, UK

ARTICLE INFO

ABSTRACT

Rotary ultrasonic machining (RUM) has been considered as an effective approach in the manufacturing of advanced materials such as ceramic matrix composite (CMC). However, the distinct removal mechanisms in RUM with different vibration forms has not been elucidated, which hinders the adoption of RUM technology in the field of material processing. In this research, the ultrasonic-assisted scratching tests of CMC were conducted to reveal the fundamentals of material removal and surface formation. Based on the kinematics of RUM processes, the vibration effects exerted in cutting areas were clarified as impact-separation and reciprocating-polishing, thus two types of diamond indenters have been specially designed for the intermittent and continuous scratching tests, respectively. The scratching force, friction factor and grooves morphology have been analyzed and compared with that of the conventional scratching without vibration. For the intermittent scratching with vertical vibration, it was found that the high frequency impact-separation between indenter and workpiece increased the critical penetration depth of ductile-brittle transition, which can help restrain the cracking defects of CMC. For the continuous scratching with tangential vibration, the overlapping rate was firstly proposed to evaluate the effect of reciprocating polishing. It was shown that higher overlapping rate and larger dynamic shear angle can be achieved by matching the scratching velocity with vibration frequency, which is conducive to obtaining even fiber fracture and better surface integrity. Due to the minimal volume of material removed in each vibration cycle, the scratching resistance was significantly lowered with smaller fluctuation under both vibration forms. Moreover, the diminishing of vibration effectiveness at certain scratching parameters was also discussed. This research work brings in a better understanding on the material removal mechanisms under different effects of ultrasonic vibration, which can provide a guidance for the design and optimization of the vibration assisted processing of advanced materials.

1. Introduction

Hard and brittle materials, like ceramics, composites and optical glasses, have superior properties and are widely used in various fields. For example, the carbon fiber reinforced SiC matrix composites (C/SiC) are generally used for the critical parts of thermal protection or high-speed braking (Naslain, 2004), due to the low density, high specific strength, excellent high-temperature ablation resistance and high wear resistance (Msaoubi et al., 2015). The machining processes of these parts after the near-net-shape fabrication are still essential to achieve the desired surface quality and dimensional accuracy for application.

However, the high hardness, high strength, and anisotropic properties lead to large cutting force (Teti, 2002), sever tool wear (Diaz et al., 2019), processing defects and surface damage in the conventional machining of these materials (Diaz and Axinte, 2017). Consequently, the application of the advanced materials is hampered by their poor machinability. Studies have shown that rotary ultrasonic machining (RUM) is an effective technology for hard and brittle materials with improved surface quality (Ning et al., 2015) and reduced tool wear (Gong et al., 2010). Various processing approaches based on RUM including milling, grinding, filing and drilling have been developed for the machining of specific geometric features, such as flat surfaces, slots,

holes, angles, etc. In these processes, there are different ultrasonic vibration effect forms working in the cutting areas, including impact-separation and reciprocating-polishing, according to the intermittent or continuous interaction between cutting tool and workpiece. The material removal mechanisms in these processes have been generally studied.

The effect of impact-separation usually exists in the surface milling and hole drilling processes using axial or vertical vibration. Pei et al. (1995) firstly proposed the rotary ultrasonic face milling (RUFM), a conical tool was used in the process to decompose the axial vibration into two components including one in axial and one in the feed direction (Pei and Ferreira, 1999). The abrasives on the conical surface of cutting tool impact and disengage from the workpiece material with high frequency (16 kHz–50 kHz) in the cutting areas. Li et al. (2005) showed that the same interaction existed in the rotary ultrasonic drilling (RUD) between the bottom surface of core drill and workpiece, due to fact that, the axial vibration is parallel with the drilling feed direction and vertical to the cutting surface (Ding et al., 2014). Therefore, the ultrasonic vibration effect in milling and drilling process can be characterized by intermittent cutting. The material removal mechanisms were mainly considered as cracks propagation and material peeling off induced by the impact and indentation of abrasives. Based on this, the theoretical models of RUFM and RUD for brittle materials including C/SiC (Li et al., 2018), ceramics (Liu et al., 2012) and CFRP (Wang et al., 2020) were established to predicted and controlled cutting force. The basic principle of these models for RUM with intermittent machining was to calculate the average impulse force of abrasives in a single cycle of ultrasonic vibration. However, the kinematic conditions to achieve intermittent cutting have not been considered in the modeling. Further investigations are still needed to understand the material removal and surface formation mechanisms during the intermittent RUM.

Another typical ultrasonic vibration effect form in RUM is the continuous reciprocating-polishing in the cutting areas. This characteristic generally exists in the ultrasonic grinding and filing process because the vibration is vertical to the feed direction and parallel to the machining surface. The ultrasonic grinding (Wang et al., 2014) and filing (Wang et al., 2016) are conducted on the advanced ceramic and C/SiC using various tools. It was found that the abrasives had no separation from the workpiece during the ultrasonic assisted machining. In addition, the trajectory length of cutting tool in contact with the workpiece was longer in RUM than that in conventional machining. Therefore, the material was removed by reciprocating cutting and polishing with continuous contact during RUM, which is distinct with that of the intermittent machining. The cutting force modeling for this process as reported by Bertsche et al. (2013) and Yuan et al. (2016), aimed to obtain the average chip thickness of a single abrasive by the simultaneous solution of macro and micro material removal rate based on the analysis of reciprocating trajectories (Brecher et al., 2010). However, the effect of reciprocating-polishing in the cutting area on the surface formation has not been evaluated (Amin et al., 2017).

To understand the mechanisms of RUM more clearly, the conventional scratching (CS) and ultrasonic-assisted scratching (UAS) tests with single abrasive were commonly conducted by other researchers. Zhang et al. (2013) investigated the groove morphology and residual stress of sapphire induced by UAS, showing that the material removal mechanism tends to be more ductile and without cracks when the ultrasonic vibration is applied. Lv et al. (2013) carried out the UAS tests on optical glass to study the surface formation mechanism and evaluated ultrasonic vibration effect on the surface roughness and cutting force during RUM. These scratching tests demonstrate that the additional ultrasonic vibration changes the interactions between abrasive and workpiece material, and thus the surface formation mechanisms. Zhou and Zhao (2016) defined the critical cutting depth of ductile-brittle transition for optical glass by UAS and it was revealed that ultrasonic vibration can reduced scratch loads and inhibited the micro-crack propagation. Feng et al. (2014) explored the material removal

characteristics of SiCp/Al in the UAS and compared the scratch load, friction coefficient and scratch morphology with that of CS. Zheng et al. (2018) worked on UAS testing of SiCp/Al, and showed that the higher material removal rate and better surface integrity can be achieved in scratching with ultrasonic vibration. Li et al. (2019) studied the influence of conventional scratching parameters on the fiber fracture of C/SiC in transverse and longitudinal scratching directions, and found that the fiber breakage and fiber/matrix interfacial debonding exhibit predominant damage behaviors. Two-dimensional UAS tests were carried out to study the material removal mechanisms in elliptical ultrasonic grinding. Cao et al. (2014) conducted the elliptical UAS on SiC to analyze the groove morphology and force ratio, and observed that the critical scratching depth for ductile mode increased more than 50 % and the scratching resistance was significantly lower compared with that of CS. Liang et al. (2013) studied the ductile-brittle transition mechanism of sapphire by elliptical UAS and obtained a larger critical cutting depth as the ultrasonic amplitude increased. However, the distinct effects of ultrasonic vibration with different vibration forms have not been evaluated and clarified.

From the review above, the most important difference among these RUM processes are the different effect forms of ultrasonic vibration in the cutting areas, hence the corresponding material removal and surface formation mechanisms are also distinct. The scratching tests can help understanding the material removal behaviors in RUM processes. However, there was no comprehensive research to clarify the influence of different vibration forms on surface formation mechanisms in UAS, and the underlying principles to achieve vibration effectiveness in RUM are still unclear. These fundamentals are critical for the process design and optimization in the RUM of difficult-to-machining materials to improve machining efficiency and quality. In this paper, two kind of indenters were designed for the intermittent and continuous UAS of CMC, respectively. The corresponding scratching force, friction coefficient and scratching grooves morphology were analyzed, and the effects of ultrasonic vibration forms, including impact-separation and the reciprocating-polishing were then studied focusing on the ductile-brittle transition and surface overlapping rate during scratching. The undermining of vibration effectiveness under given scratching parameters was also discussed.

2. Experimental method

The ultrasonic-assisted scratching (UAS) tests were performed on a 3-axis vertical machining center with an in-house designed ultrasonic vibration device. As shown in Fig. 1a, the experimental setup has four main parts: an ultrasonic vibration system, a diamond scratching indenter, material sample and the 3-axis dynamometer (9257B, Kistler). The ultrasonic vibration system was mounted on the machine spindle and drove the scratching indenter with the axial vibration, operating at a frequency of 17 kHz with an amplitude of 5 μm. According to the kinematic analysis of typical RUM processes, two components of ultrasonic vibration act in the cutting area in the form of impact-separation and reciprocating-polishing. Therefore, to analyze the distinct effect of the two vibratory components, the diamond indenters with a face angle of 90° and a nose radius of 10 μm were designed for these two vibration forms, i.e. intermittent and continuous scratching. This is shown in Fig. 1c, d where, the vibration of the bottom indenter is perpendicular to the workpiece surface, while the side indenter can transfer the axial vibration to be parallel to the scratching surface. This allows to achieve distinct material removal and surface formation mechanisms.

Carbon fiber reinforced SiC matrix composites (C/SiC), with 2.5D needled structure, fabricated by precursor infiltration pyrolysis (PIP) were chosen for the tests. The C/SiC samples were cut using abrasive waterjet into the size of 10 mm × 10 mm × 5 mm, and then the samples were polished to control the surface roughness within Ra 100 nm. The prepared sample was fixed on the dynamometer by heat-softened glue and the dynamometer was mounted on the machine table. Stainless steel
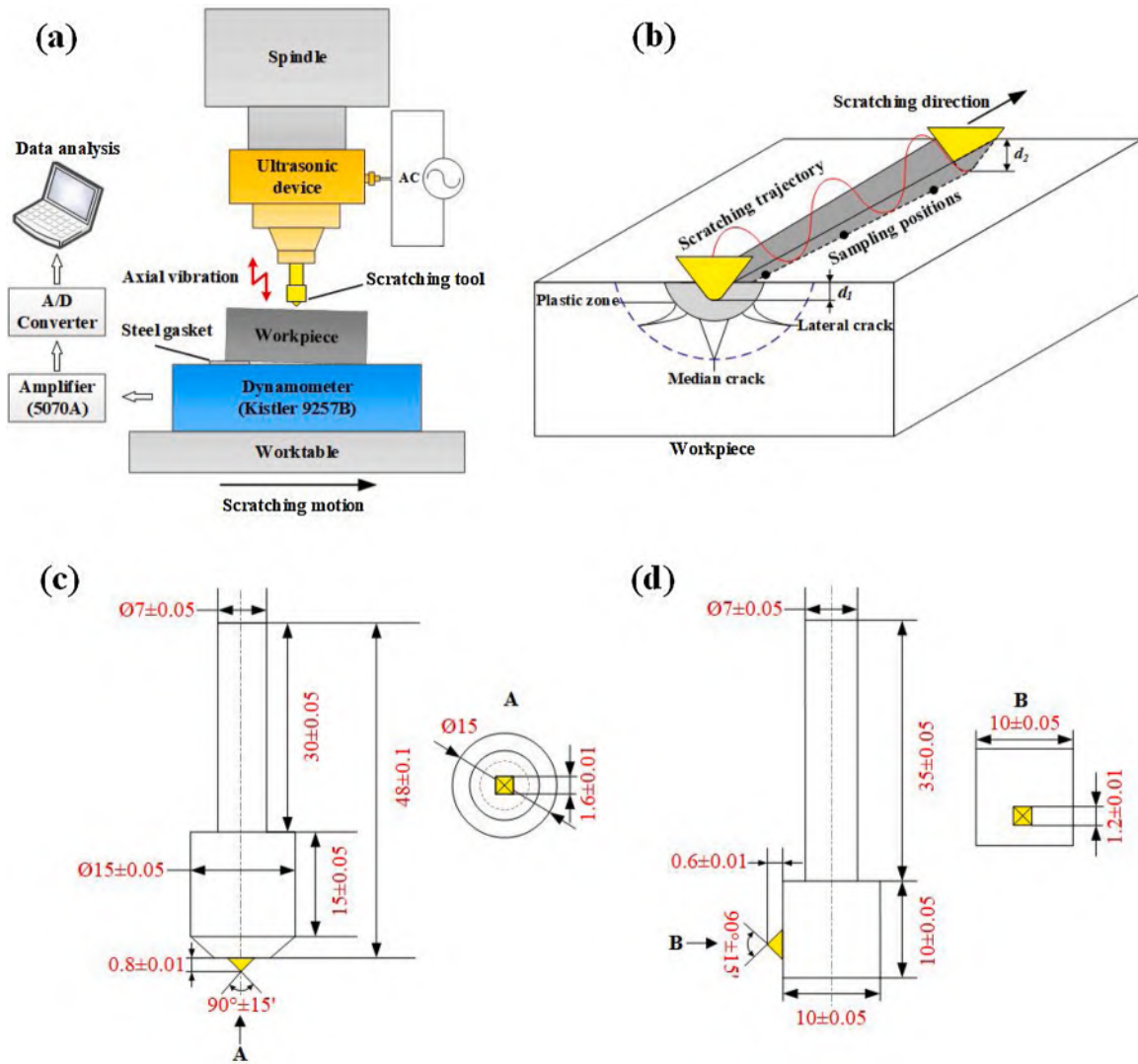
Fig. 1. (a) Schematic diagram of UAS test. (b) The formation of groove on workpiece by UAS and the sampling detection of groove morphologies. (c) The bottom indenter designed for intermittent scratching test. (d) The side indenter designed for continuous scratching test.

gaskets with a thickness of 10 μm were used to adjust the slope of the workpiece, inducing an angle to achieve an oblique scratching test. This allows to secure the scratching depth linearly increasing from 0 to 10 μm along the scratching length of 10 mm. A micrometer gauge was used to square the workpiece position to ensure that the scratching depths were identical in all tests. The scratching motion of the indenter was achieved by the movement of worktable, and the horizontal scratching velocity varied from 60−7500 mm/min. The dynamic normal and tangential forces during scratching tests were measured by the 3-axis dynamometer, and the corresponding friction factor was then calculated. The morphologies of the scratching grooves at different scratching depth and velocity were detected and analyzed by scanning electron microscope (SEM) as shown in Fig. 1b. The conventional scratching (CS) tests without vibration were conducted as control experiments on the same sample with a interval of 1.5 mm. It should be noted that in the practical RUM processes, the material removal can be simplified as multiple scratching at the same groove, and due to the superposition effect of multiple scratching and feed motion, the ultrasonic vibration has no significant influence on scratching depth. Therefore, in the single scratching using the bottom indenter, the initial distance between the indenter and workpiece was increased by an vibration amplitude to compensate the influence of ultrasonic vibration on the scratching depth.

3. Results and discussion

3.1. Intermittent scratching test by UAS

One of the typical ultrasonic vibration effects in the cutting area during RUM is the intermittent machining behavior, which induces the features of impact-separation. To study the effects of this vibration form on material removal and surface formation, the intermittent scratching tests of C/SiC were conducted with ultrasonic vibration, as shown in Fig. 2, the bottom indenter was used to transfer the vibration vertical to the polished workpiece surface, this allows the indenter to periodically penetrate into and disengage from the C/SiC sample with high frequency (17 kHz) during scratching. Comparing with the conventional scratching, the scratching trajectory and penetration depth are dynamically changing in the intermittent scratching, inducing a distinct material removal mechanism. The study of intermittent scratching was carried out focusing on the theoretical analysis, scratching morphology and scratching force.

3.1.1. Theoretical analysis of intermittent behavior

The kinematics of the vibratory scratching with a vibration frequency f and amplitude A is schematically shown in Fig. 3. Here, the bottom indenter penetrates into the workpiece for a certain time (ΔT)
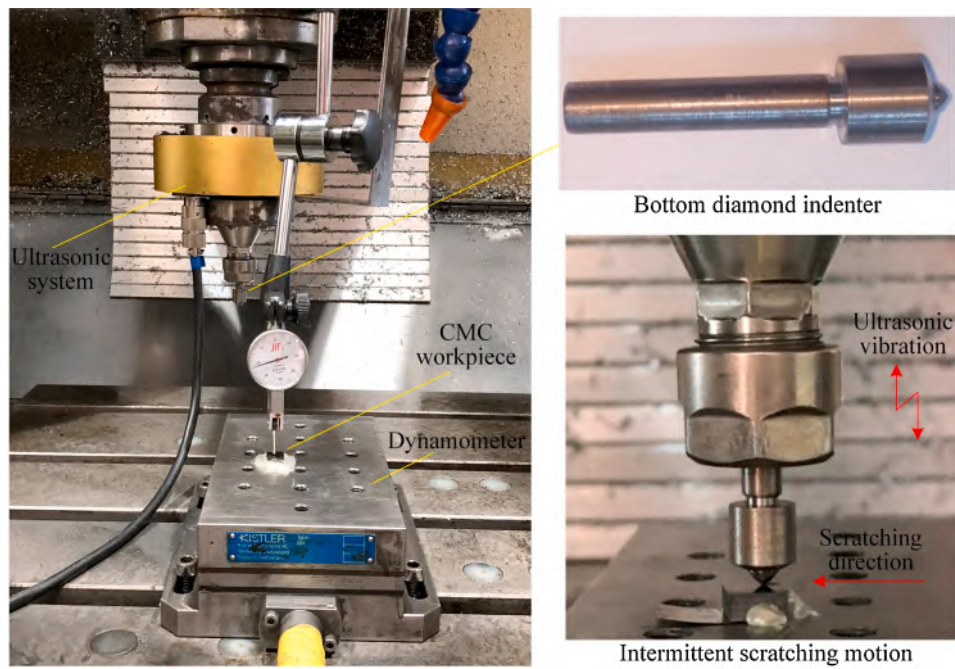
Fig. 2. Intermittent scratching test assisted by vertical ultrasonic vibration.
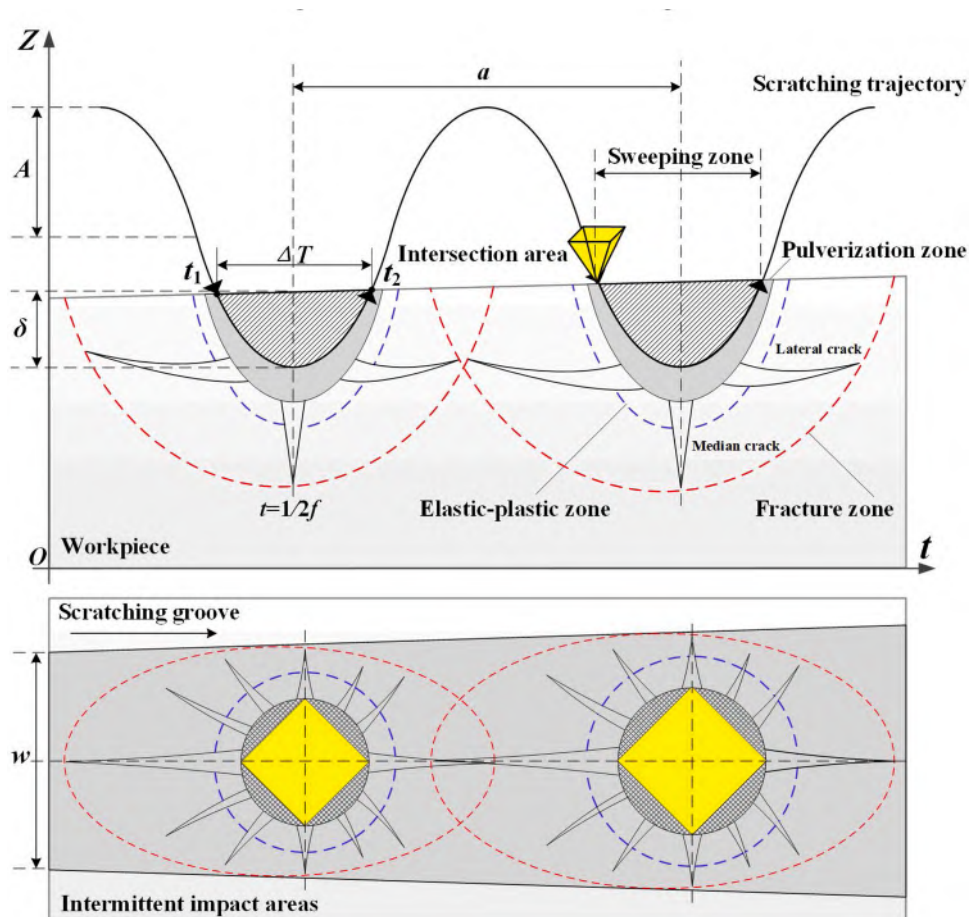

Fig. 3. The intermittent scratching behavior induced by ultrasonic vibration.

and disengage from the workpiece during one vibration cycle, thus the penetration depth of the indenter (δ) changes periodically from zero to the maximum value at the peak of the vibration. According to Hertz contact theory, the material deformation and cracks initiation during scratching are significantly affected by the normal penetration force. The material removal mechanism tends to transit from ductile removal to brittle fracture at the critical penetration depth. Therefore, the superimposed ultrasonic vibration will change the response characteristics of the material during the intermittent scratching.

During a single vibration cycle in Fig. 3, the indenter comes in contact with the workpiece material at a time t_1 ($\delta = 0$). Subsequently, along with the scratching motion, the penetration depth increases to the maximum ($\delta=\delta_{mn}$) at the vibration peak ($t = 1/2f$). Then, the indenter retracts gradually up to ($\delta = 0$) at a time t_2. The dynamic change of the penetration depth during the effective scratching time (ΔT) can be expressed as:

$$\begin{cases} \delta = \delta_{max} - (A\cos(2\pi f t) + A)t \in [t_1 - t_2] \\ t_1 = \dfrac{\arccos\left(\dfrac{\delta_{max}}{A} - 1\right)}{2\pi f} \\ t_2 = \dfrac{2\pi - \arccos\left(\dfrac{\delta_{max}}{A} - 1\right)}{2\pi f} \end{cases} \tag{1}$$

The instantaneous cutting force $F_n^{'}$ during the impact cycle can be expressed as (Li et al. (2018)):

$$F_n{'} = 4k_1 \frac{\tan\alpha}{\cos\alpha} \cdot H_v \cdot \delta^2 \tag{2}$$

k_1 is a correlation factor of indenter shape. α is the half angel of the diamond indenter. H_v is the Vikers-hardness of workpiece material.

Therefore, the impulse of the scratching force during one vibration cycle can be computed as:

$$I = \int_0^{1/f} F_n{'} dt = \int_{t_1}^{t_2} F_n{'} dt \tag{3}$$

The sinusoid of penetration trajectory with high vibration frequency as shown in Fig. 3 can be simplified into the forms of straight lines, and can be approximated as:

$$\begin{cases} \delta = \dfrac{\delta_{max}}{1/2f - t_1} t - \dfrac{\delta_{max}}{1/2f - t_1} t_1 t \in \left[t_1 - \dfrac{1}{2f}\right] \\ \delta = \dfrac{\delta_{max}}{1/2f - t_2} t - \dfrac{\delta_{max}}{1/2f - t_2} t_2 t \in \left[\dfrac{1}{2f} - t_2\right] \end{cases} \tag{4}$$

The substitution of Eqs. (2) and (4) into Eq. (3), gives:

$$I = 2\int_0^{\delta_{max}} 4k_1 \frac{\tan\alpha}{\cos\alpha} \cdot H_v \cdot \delta^2 \cdot \left(\frac{1/2f - t_1}{\delta_{max}}\right) d\delta = \frac{8}{3}k_1 \cdot \frac{\tan\alpha}{\cos\alpha} H_v \cdot (1/2f - t_1)\delta_{max}^2 \tag{5}$$

The average penetration force of the indenter within one vibration cycle can be obtained as:

$$F_n = I \cdot f = \frac{4k_1}{3\pi} \cdot \frac{\tan\alpha}{\cos\alpha} H_v \cdot \left(\pi - \arccos(\frac{\delta_{max}}{A} - 1)\right)\delta_{max}^2 \tag{6}$$

The critical load applied on brittle material causing cracks can be expressed as (Lawn et al. (1980)):

$$P_c = k_2 \frac{K_{IC}^4}{H_v^3} \tag{7}$$

k_2 is a correlation factor of the indenter shape. K_{IC} is the fracture toughness of workpiece.

Therefore, the critical penetration depth (δ_{cu}) for ductile removal under ultrasonic vibration during intermittent scratching can be given by the solution of Eqs. (6) and (7):

$$\frac{4k_1}{3\pi} \frac{\tan\alpha}{\cos\alpha} H_v \left(\pi - \arccos(\frac{\delta_{cu}}{A} - 1)\right)\delta_{cu}^2 = k_2 \frac{K_{IC}^4}{H_v^3} \tag{8}$$

While, in the conventional scratching (CS) without vibration, according to Eqs. (2) and (7), the critical penetration depth (δ_{cc}) can be expressed as:

$$4k_1 \frac{\tan\alpha}{\cos\alpha} H_v \delta_{cc}^2 = k_2 \frac{K_{IC}^4}{H_v^3} \tag{9}$$

Simultaneously solving Eqs. (8) and (9), the ratio of the critical penetration depth in intermittent scratching to that in the CS can be obtained:

$$\frac{\delta_{cu}}{\delta_{cc}} = \sqrt{\frac{3}{1 - \frac{1}{\pi}\arccos\left(\frac{\delta_{cu}}{A} - 1\right)}} \tag{10}$$

It can be seen from Eq. (10) that the due to the additional ultrasonic vibration, the critical penetration depth (δ_{cu}) in the intermittent scratching will increase by over 70 %, comparing with the conventional scratching (δ_{cc}). In addition, when δ_{cu} is less that the vibration amplitude A, the indenter can completely disengage from the scratching surface, producing the high frequency impact-separation with workpiece material. And then acrcos(δ_{cu}/A-1) is over $\pi/2$, and the δ_{cu} will increase to be more than 2 times of δ_{cc}, indicating that the effect of impact-separation under ultrasonic vibration is benefit to achieve the ductile removal mode during scratching, and thus the initiation and propagation of cracks will be inhibited, which have been also found in other high strain rate machining of brittle materials by (Zhang and Yin, 2019) and (Yang and Zhang, 2019). Therefore, theoretically, the intermittent scratching of C/SiC assisted with ultrasonic vibration can decrease the surface cracks and interface defects as well as fiber fracture.

3.1.2. Intermittent scratching morphology

The formation of the scratching morphology is the result of the intermittent interaction between indenter and workpiece material, as schematically illustrated in Fig. 3. According to the solid fracture theory (Orowan, 1949), the plastic deformation area appears first at the impact area when the indenter penetrates into the material. Since the material is brittle, and the strain rate is extremely high for the material to display its plasticity, the deformation switches into brittle mode and induced a crushed zone with pulverization particles as well as an elastic-plastic zone around the indenter. With the increase of penetration depth, the median cracks grow, and then the cracks close when unloading, generating the lateral cracks near the free surface. The lateral cracks extend and intersect with each other between the adjacent impact areas. Thus, the scratching of the indenter will induce peeling of the workpiece material. Due to the tensile stress of scratching motion behind the indenter, the lateral cracks tend to be longer behind the indenter, which reinforces the peeling effect.

Therefore, the distance between the adjacent impact areas (a) determines the range of the intersection area and its morphology, it can be expressed as $a=v/f$, and v is the scratching velocity. The intermittent scratching morphologies for different scratching velocity at the same depth of 2 μm are displayed in Fig. 4. It can be seen that, as v increased from 60 mm/min to 7500 mm/min, the adjacent impact distance a changed from about 0.06 μm–7.4 μm. Therefore, at low scratching velocity, there are more impacts hammering at a unit length and the material was then effectively removed in the intersecting impact areas, thus the scratching grooves tended to be wide and deep as shown in Fig. 4a,b. With higher scratching velocity, the number of impacts per unit scratching length decreased as the impacts are spaced with a larger distance. Therefore, the superimposed vibration was diluted during scratching and the residual material between the adjacent impacts was not fully removed, as shown in Fig. 4c, d. This indicates that one should select carefully the cutting velocity in the intermittent RUM processes,
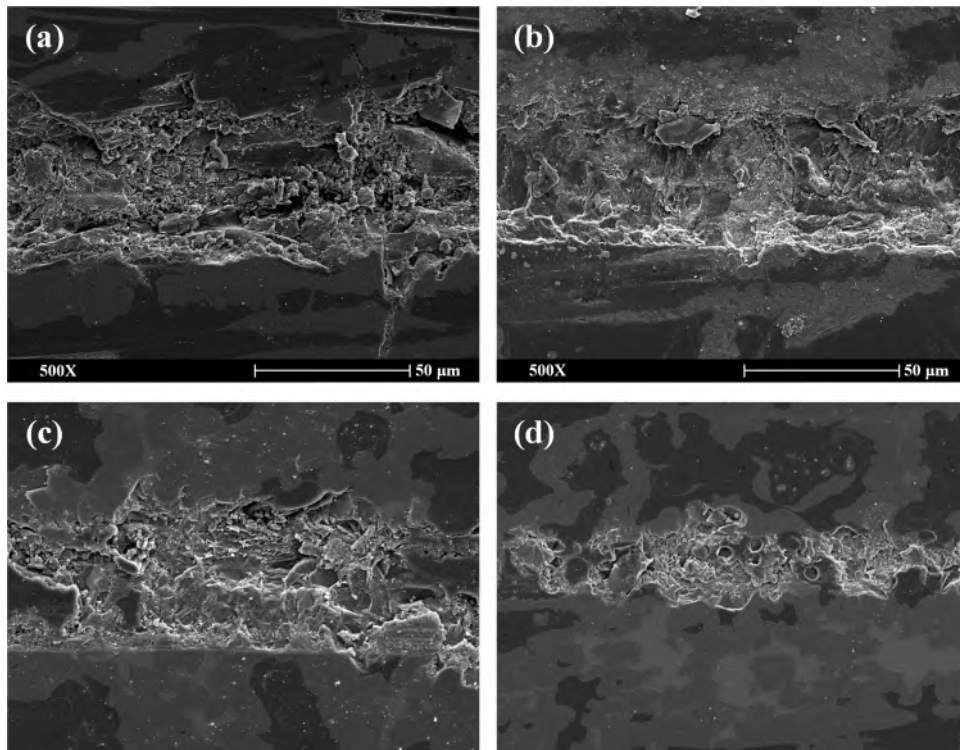
Fig. 4. Intermittent scratching morphologies at different scratching velocity, (a) $v = 60$ mm/min, (b) $v = 300$ mm/min, (c) $v = 1500$ mm/min, (d) $v = 7500$ mm/min.

since high cutting velocity may undermine the effectiveness of ultrasonic vibration. Hence, the cutting velocity during the intermittent machining need to be matched with the vibration frequency based on the crack propagation behaviors and material fracture properties, aiming to sufficiently exploit the advantages of ultrasonic vibration in RUM.

The comparison of conventional and intermittent scratching morphology at different depth is given in Fig. 5, where the scratching velocity was selected as 300 mm/min to fully remove the materials on the scratching path. Based on the indentation theory, when the scratching depth δ is less than the critical depth δ_C, the material is mainly removed through ductile flow without large cracks. However, when δ increases to be greater than δ_C, intensive cracks around the scratching groove will be generated. It is observed in Fig. 5b that, when $\delta < 1$ μm, the scratching morphology on C/SiC appeared as plastic flow marks in the intermittent scratching, while a few of cracks were initiated in the conventional scratching (Fig. 5a). As the scratching depth increasing to 2 μm, the material was mainly removed by brittle spalling in the conventional scratching, leading to the craters and cracks on the grooves (Fig. 5c). However, the ductile plowing marks can still be observed in the scratching assisted by ultrasonic vibration in Fig. 5d, which supports the theoretical analysis in Eq. (10). With further increase of scratching depth to 4 μm, the carbon fibers in C/SiC were severely fractured and detached from the SiC matrix by the shearing and indentation in scratching as illustrated in Fig. 5e. However, when applying the ultrasonic vibration, the fibers and interfaces around the scratching grooves exhibited better integrity as shown in Fig. 5f. This is because the fiber fracture and crack propagation were localized in a small area by each scratching cycle of high frequency vibration, which significantly reduced the processing defects.

3.1.3. Scratching force and friction factor

The dynamic change of normal force (Fz) and tangential force (Fx) along with the scratching of C/SiC at $v = 300$ mm/min is shown in Fig. 6a, b, and the dynamic friction factor (Fx/Fz) during scratching is calculated in Fig. 6c. Comparing with the CS (conventional scratching) test, the intermittent scratching force achieved 30 % reduction on

average with the assistance of ultrasonic vibration, and the corresponding friction factor (0.22 on average) was also lower than that in CS (0.37 on average). This can be explained that the impact-separation at high frequency during intermittent scratching decreased the contact time between indenter and workpiece material, thus it produced shorter chips, leading to lower scratching load and friction on indenter. Meanwhile, the minimal volume of material removed by each vibration cycle effectively restrained the material fracture and large cracks propagation, and the proportion of ductile removal during scratching was then increased, which is supported by the aforementioned morphology analysis. Therefore, it can be seen in Fig. 6 that the intermittent scratching force tended to be more stable, especially in the range of small scratching depth, at which the material tended to be removed by ductile mode with less initiation of random cracking during scratching. In contrast, the scratching force in CS appeared more fluctuations, due to the acting load induced by the instable removal behaviors like fiber fracture and interface debonding. The variation of scratching force further verified the surface formation mechanism during the intermittent scratching.

According to the kinematics of intermittent scratching, the relation between the scratching depth and ultrasonic amplitude ($A = 5$ μm) can significantly affect the separation behavior between indenter and workpiece material, which will further affect the effectiveness of ultrasonic vibration and change the scratching load. As shown in Fig. 7, when the scratching depth (δ) was below 6 μm, it was close to or less than the ultrasonic amplitude, thus the indenter can completely disengage with workpiece material, achieving the feature of intermittent scratching, then the corresponding resultant load was reduced by over 35 % comparing with the CS. However, when the scratching depth was greater than ultrasonic amplitude, the indenter cannot fully separate with the workpiece during scratching, thus the intermittent behavior was diminished, and the reduction rate of scratching load decreased to 20 %. Therefore, to make better use of the advantages of ultrasonic vibration in the practical RUM, the cutting depth of abrasives should be comparable to the vibration amplitude to obtain the intermittent characteristic in the cutting area.
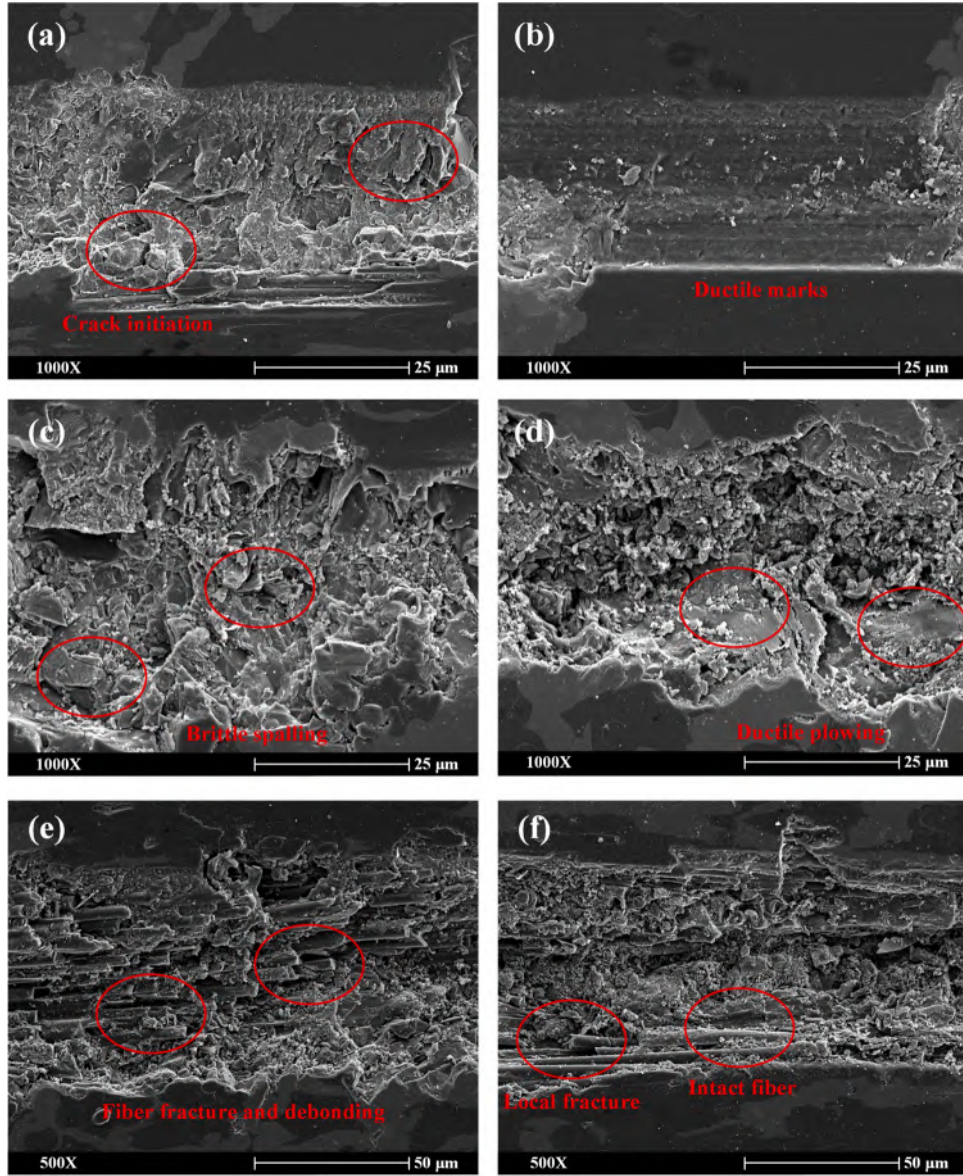
Fig. 5. Scratching morphology of CS in (a), (c), (e), and intermittent UAS in (b), (d), (f) at different scratching depth. (a), (b) are in δ=0.6-1 μm. (c), (d) are in δ=1.6-2 μm. (e), (f) are in δ=2.4-4 μm.

Therefore, in the practical RUM processes characterized by impact-separation behavior, the cutting depth of abrasives (d), which is in direct proportion to the feed per revolution ($d \propto 60v_f/S$), should be set comparable to the vibration amplitude (A) to obtain the intermittent cutting behavior. Besides, the cutting speed ($v=\pi SR/30$) should not be over high, so as to ensure the sufficient impact times per cutting length ($n=f/v=30f/\pi SR$). The cutting parameters in RUM should be matched as follows:

$$\begin{cases} A > d \propto 60v_f/S \\ n = 30f/\pi SR > N \end{cases} \tag{11}$$

A is the vibration amplitude, f is the vibration frequency, d is the cutting depth of abrasives, v_f is the feed velocity in RUM, S is the spindle revolution per minute (rpm) in RUM, n is the impact times per cutting length, R is the cutting tool diameter, N is the critical impact times per cutting length that can fully remove materials. Thus, the cutting parameters and ultrasonic vibration parameters in RUM can be adjusted according to Eq. (11) to eliminate the diminishing effect of ultrasonic vibration, as demonstrated in the RUFM experiments (Li et al. (2018)).

3.2. Reciprocating scratching test with UAS

Another typical effect form of ultrasonic vibration exerted in the cutting area during RUM is the continuous contact along with reciprocating-polishing. To simulate these vibration features, the continuous scratching tests of C/SiC assisted with ultrasonic vibration have been carried out, as shown in Fig. 8, the side indenter was utilized and the workpiece was fixed on the side surface of the dynamometer, transferring the axial ultrasonic vibration to be parallel with the workpiece surface. Thus, the indenter achieved the reciprocating vibration in the scratching plane, this scratching kinematics led the scratching trajectory to be a sine curve around the scratching direction, producing the reciprocating-polishing effect on the grooves. The following discussion will focus on the effect of lapping and polishing induced by tangential vibration during scratching.

3.2.1. Overlapping rate of reciprocating polishing

Comparing with the conventional scratching (CS), the scratching trajectory and the interaction with workpiece material are distinct
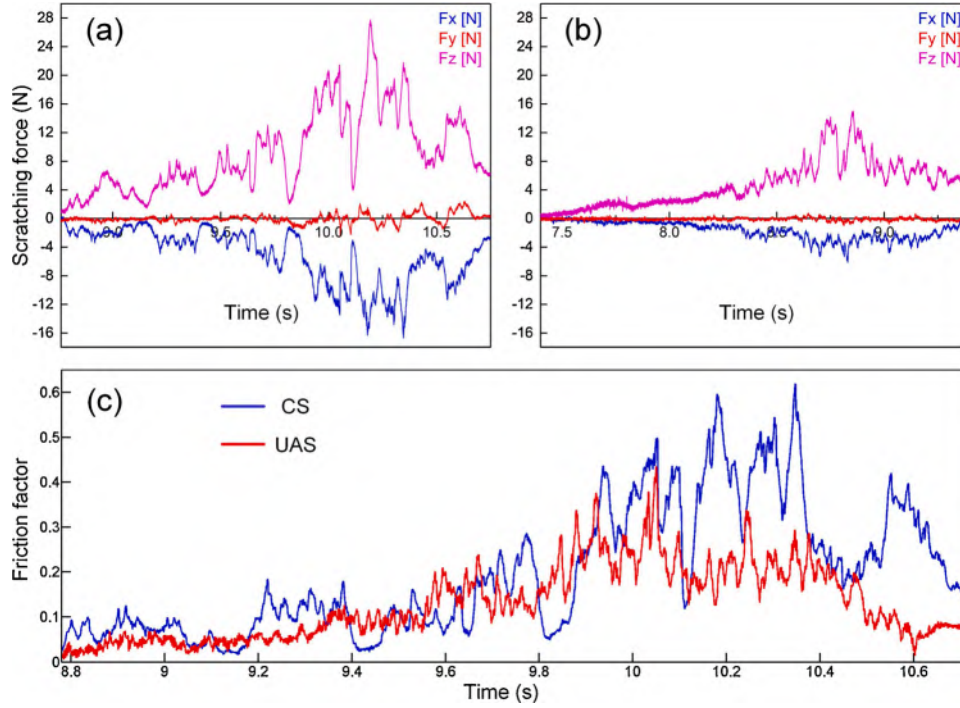
Fig. 6. The variation of scratching force in (a) conventional scratching (CS), (b) intermittent scratching assisted by ultrasonic vibration (UAS). (c) The comparison of friction factor.
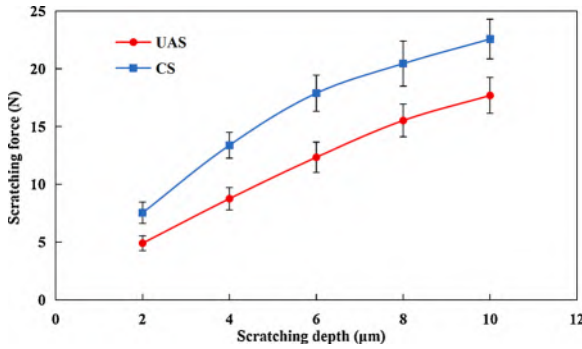

Fig. 7. The influence of scratching depth on the resultant force of scratching.

during the continuous UAS scratching, as schematically illustrated in Fig. 9. It is seen that the trajectory length of continuous scratching (l_u) is greater than that of CS (l_c) in the scratching direction. The trajectory of l_u can be simplified as straight lines marked in red in Fig. 9a. Therefore, according to the scratching kinematics, the ratio of trajectory length in one vibration cycle can be approximated as:

$$\frac{l_u}{l_c} = \sqrt{1 + \left(\frac{4Af}{v}\right)^2} \qquad (12)$$

In the practical machining of brittle materials, at the same machining parameters or material removal rate, the longer cutting trajectory will lead to smaller contact area between cutting tool and workpiece material as well as the smaller average cutting depth, which can achieve higher machining quality without compromise of efficiency. It can be seen from Eq. (12) that the trajectory length increased with vibration amplitude and frequency, but a high scratching velocity will diminish this benefit. Meanwhile, in the direction vertical to scratching, the width of the continuous scratching grooves (w_u) can be increased by twice amplitude of ultrasonic vibration than the conventional scratching width (w_c), as shown from the section view in Fig. 9b. These interactions

between indenter and workpiece material lead to the repeated scratching around the scratching path, as shown in Fig. 9a. Due to the penetration width of indenter, the scratching trajectories overlap with each other along with the ultrasonic vibration, producing reciprocating-polishing effect on the scratching grooves. This effect can help remove the residual or cracked material debris from the groove surface, thus achieving better surface integrity.

Based on the kinematic analysis of the continuous scratching in Fig. 9, it can be obtained that the reciprocating-polishing effect is significantly influenced by the wave length of the scratching trajectory (λ) and the penetration width (w). The trajectories overlapping behaviors can be divided into several conditions according to different scratching parameters, as shown in Fig. 10, in a single vibration cycle, when $w < \lambda/2$, the scratching trajectory will bypass the residual areas (RA) as the indenter sweeping over the workpiece surface, thus the material around the scratching path cannot be sufficiently removed, which is detrimental to the surface quality. When $w = \lambda/2$, the material on the scratching path is just completely removed. When, w is further increased, an overlapping area on the scratching path will be formed, and the material in this area will be repeatedly scratched, which is conducive to improving surface integrity. When $w = \lambda$, the indenter sweeping of the material on the scratching path will be repeated once during a single scratching, and the repeat rate as well as overlapping area (OA) will be further enlarged when w increases to over λ, producing the reciprocating-polishing effect on the scratching grooves during the continuous scratching by UAS.

Therefore, to evaluate the reciprocating-polishing effect, the repeating scratching times of the workpiece material during the continuous scratching can be defined as the overlapping rate (O_r), which can be expressed as:

$$O_r = \frac{2w}{\lambda} - 1 \qquad (13)$$

The penetration width (w) and wavelength (λ) of scratching trajectory can be expressed as:
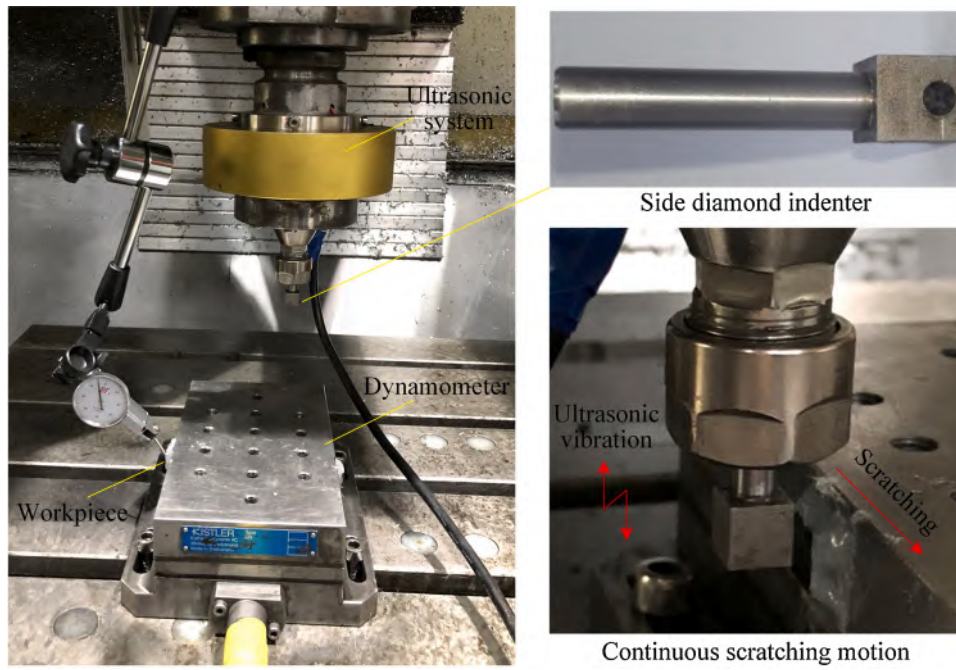
Fig. 8. Continuous scratching test assisted by ultrasonic vibration.
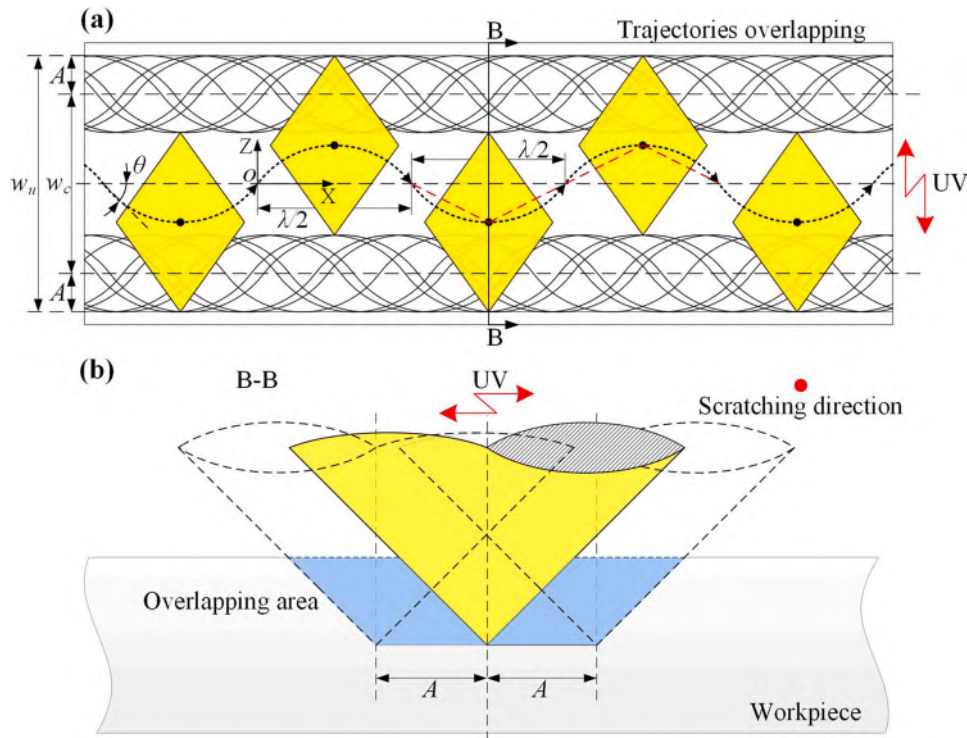

Fig. 9. Reciprocating-polishing effect in the continuous scratching by UAS. (a) The trajectories overlapping in the scratching direction. (b) Section view of the continuous scratching.

$$\begin{cases} w = 2\delta\tan\alpha \\ \lambda = v/f \end{cases} \tag{14}$$

The solution of Eqs. (13) and (14) gives the relation of overlapping rate with the scratching depth (δ), vibration frequency (f) and scratching velocity (v):

$$O_r = \frac{4\delta f\tan\alpha}{v} - 1 \tag{15}$$

The reciprocating-polishing effect is a critical characteristic of the continuous scratching by UAS. Higher overlapping rate corresponds to the enhanced reciprocating polishing, and the scratching morphology as well as scratching load will be also significantly influenced by the overlapping rate.

3.2.2. Reciprocating scratching morphology

The comparison of scratching morphology at a depth of 6 μm ob-
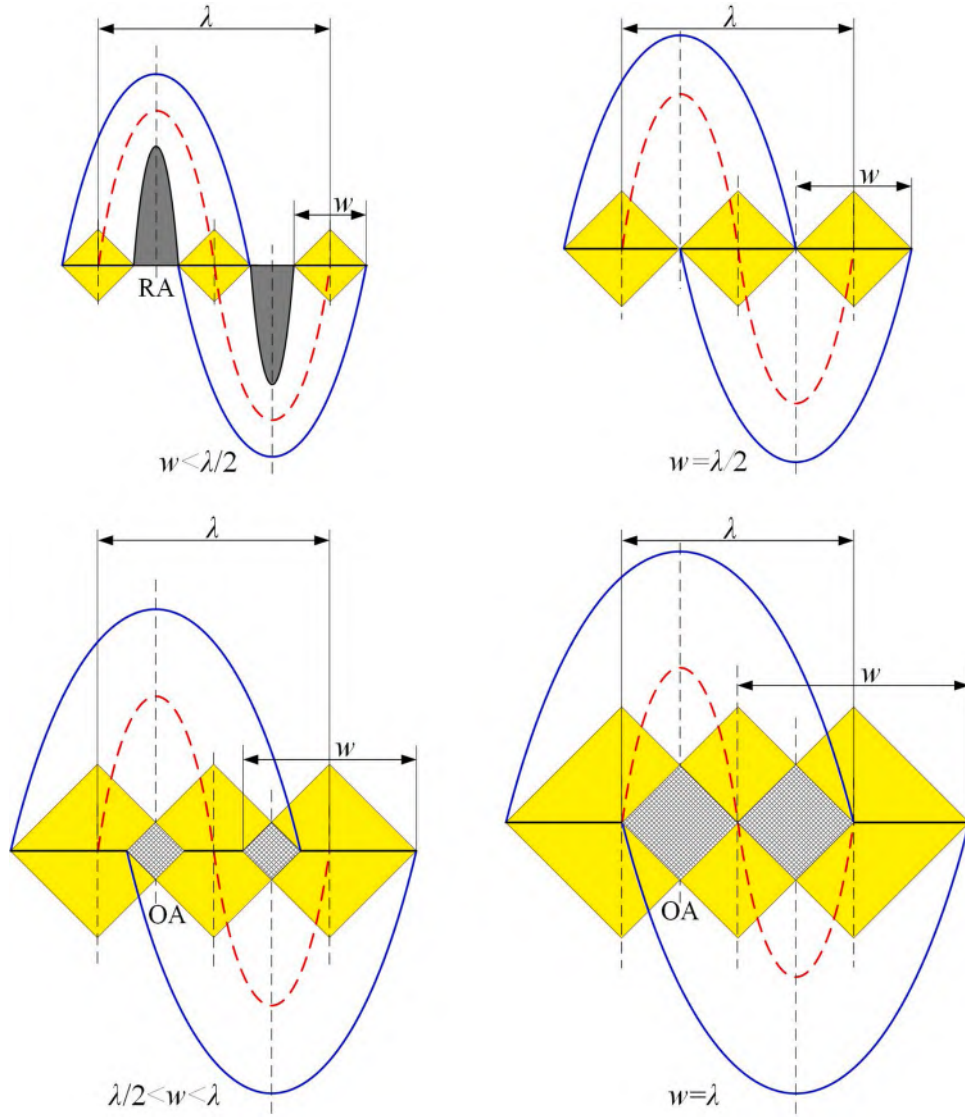
Fig. 10. The overlapping conditions during the continuous scratching.

tained by CS and continuous scratching under different scratching velocity is given in Fig. 11. It shows that the continuous scratching by UAS achieved better surface integrity of the grooves with less defects such as fiber rupture, matrix delamination and interface cracking. This supports the benefit of the reciprocating-polishing effect induced by ultrasonic vibration. Due to the reciprocating vibration of the indenter, the angle (θ) between the instantaneous scratching direction and the carbon fiber changes dynamically, as shown in Fig. 9a, the equation of scratching trajectory in the illustrated coordinate system can be derived as:

$$z = A\sin\left(\frac{2\pi f}{v}x\right) \tag{16}$$

x is the scratching length along the groove. If the fiber orientation is parallel to the macro scratching direction, then the shearing angle θ ($<90°$) will change from the maximum value (θ_{max}) at the initial position to zero at the vibration peak, and it can be deduced as:

$$\theta = \arctan(z') = \arctan\left(\frac{2\pi A f}{v}\cos\left(\frac{2\pi f}{v}x\right)\right) \tag{17}$$

Thus, with the dynamic variation of θ, the reinforcing fibers were ruptured and removed by shearing within a small range during one vibration cycle. The maximum shear angle obtained from Eq. (17) can be

expressed as:

$$\theta_{\max} = \arctan\left(\frac{2\pi A f}{v}\right) \tag{18}$$

Large shear angle θ_{max} will produce more shearing load on carbon fibers rather than pulling load during scratching (Li et al. (2019)), which is conducive to obtaining intact fibers with minimal cracks on the scratching grooves, as shown in Fig. 11b,d,f,h, it can be calculated from Eq. (18) that the corresponding θ_{max} increased from 76.8° to 89.8° as the scratching velocity v varied from 7500 mm/min to 60 mm/min, therefore the most uniform surface was achieved at the lowest scratching velocity $v = 60$ mm/min during the continuous scratching. Meanwhile, the overlapping rate (O_r), as defined in Eq. (15), also increased remarkably from 2.3 to 407 as the scratching velocity decreased from 7500 mm/min to 60 mm/min, thus the enhanced reciprocating polishing further removed the cracking layers left on the scratching grooves, leading to a better surface integrity as shown in Fig. 11b. This indicates that the high scratching velocity may undermine the effectiveness of ultrasonic vibration to improve surface quality in the continuous scratching.

In addition, as the scratching velocity increased, the degradation of scratching surface quality was observed in both scratching tests. From
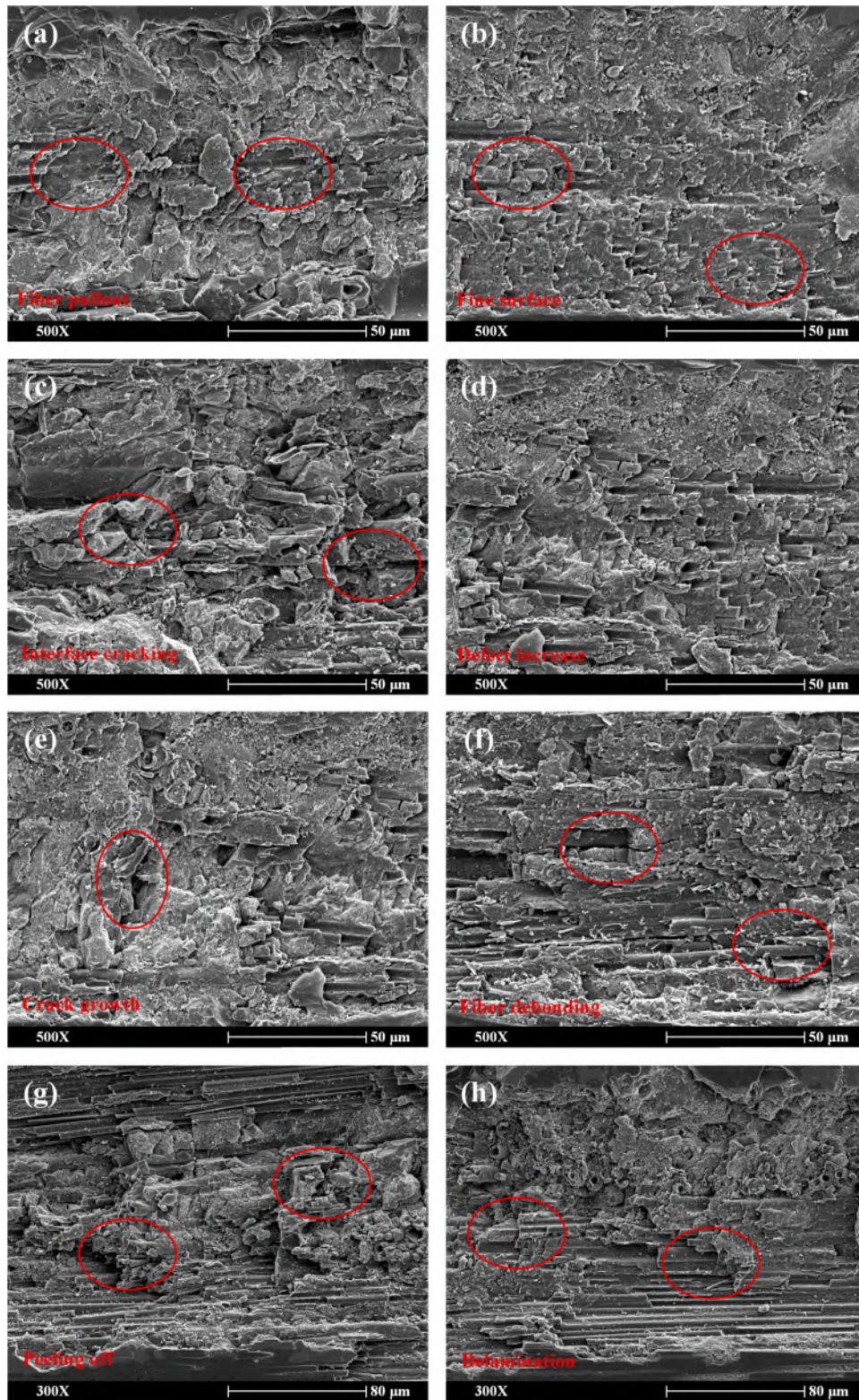
Fig. 11. Scratching morphology of CS in (a), (c), (e), (g), and continuous UAS in (b), (d), (f), (h) at different scratching velocity. (a), (b) are at *v*=60 mm/min. (c), (d) are at *v*=300 mm/min. (e), (f) are at *v*=1500 mm/min. (g), (h) are at *v*=7500 mm/min.

the perspective of energy dissipation, at low scratching velocity or strain rate, the scratching energy input into C/SiC workpiece by indenter is consumed by the localized rupture of carbon fiber bundles and SiC matrix, which is benefit to suppress the propagation of cracks in large area. While, at high scratching velocity or strain rate, the energy cannot be sufficiently dissipated by fine cracks from localized fracture, instead,

the carbon fibers and SiC matrix tended to be pulled out and torn off, as shown in Fig. 11e,f,g,h, inducing peeling off and delamination of the composite material around the scratching grooves. Therefore, in the continuous RUM of CMC materials, it is critical to select proper cutting velocity to achieve high scratching angle (θ_{max}) and overlapping rate (O_r), to guarantee the effectiveness of ultrasonic vibration and obtain

better surface quality.

3.2.3. Scratching force and friction factor

As the workpiece was fixed onto the side of the dynamometer in the continuous scratching test, the normal and tangential scratching force was converted to be Fx and Fy respectively. The dynamic force ratio factor or friction factor can be calculated as Fy/Fx, and the comparison of CS and continuous scratching load at $v = 300$ mm/min is shown in Fig. 12. With the assistance of ultrasonic vibration, the scratching force was reduced by about 40 % on average, and the corresponding mean friction factor was also decreased from 0.35 to 0.24.

On one hand, the dynamic change of the shearing angle (θ), as aforementioned in the scratching morphology discussion, led to a vertical component of scratching direction to the carbon fiber orientations, thus the fiber bundles tended to be removed by shearing fracture, which is the minimum energy consumption mode of fiber fracture rather than the pulling or bending fracture, thus the scratching resistance was significantly reduced by the reciprocating vibration. On the other hand, the reciprocating-polishing effect, as illustrated in Fig. 10, minimized the volume of material removal in each vibration cycle, due to the high overlapping rate during the continuous scratching. Moreover, the reciprocating vibration of the indenter can prevent the accumulation of the material debris on the scratching path, which also contributes to lower the scratching force and friction.

To assess the influence of overlapping rate (O_r) on the scratching load, the comparison of resultant scratching forces at different scratching velocities was also carried out, as shown in Fig. 13, O_r increased from 2.3 to 407 when the scratching velocity changed from 7500 mm/min to 60 mm/min, as expected, the resultant force of continuous scratching with UAS decreased with the increase of O_r. The CS tests as the contrast group were also conducted at the corresponding scratching velocity. It was found that the resultant force in continuous scratching was significantly reduced comparing to the CS without ultrasonic vibration, and the average reduction of the scratching force decreased from 45 % to 18 % as the overlapping rate decreased. This indicates that the effectiveness of additional ultrasonic vibration is diminished. As the scratching
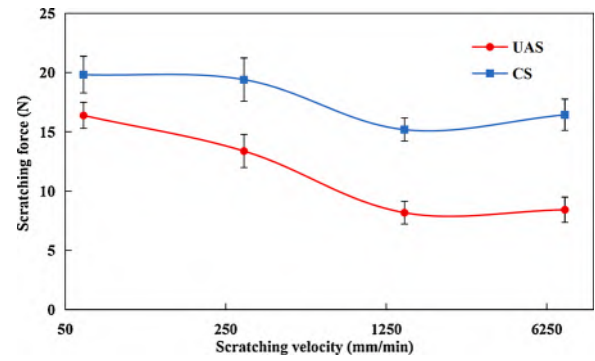

Fig. 13. The influence of scratching velocity on the resultant force of scratching.

velocity increases, the ratio of vibration amplitude to wave length (A/λ) decreases, as shown in Fig. 9, the trajectories of continuous scratching tend to be straightened, and gradually approach to the scratching trajectory in CS, thus the overlapping rate as well as the shearing angle are decreased, which is against to the scratching load reduction.

Therefore, for the RUM processes characterized by reciprocating-polishing behavior, the overlapping rate (O_r) and maximum shear angle (θ_{max}) in the cutting area can be used as comprehensive factors to evaluate and regulate the surface machining quality. According to Eqs. (15) and (18), the high vibration frequency (f) and the corresponding proper cutting velocity (v) are benefit to enhance reciprocating-polishing effect, thus improving surface integrity and decreasing cutting force in the practical RUM. Similar results have been found in the ultrasonic assisted grinding (Wang et al. (2014)) and filling experiments (Wang et al. (2016)).

4. Conclusions

To study the distinct forms of ultrasonic vibration exerted in the cutting area during RUM, two types of diamond indenters have been
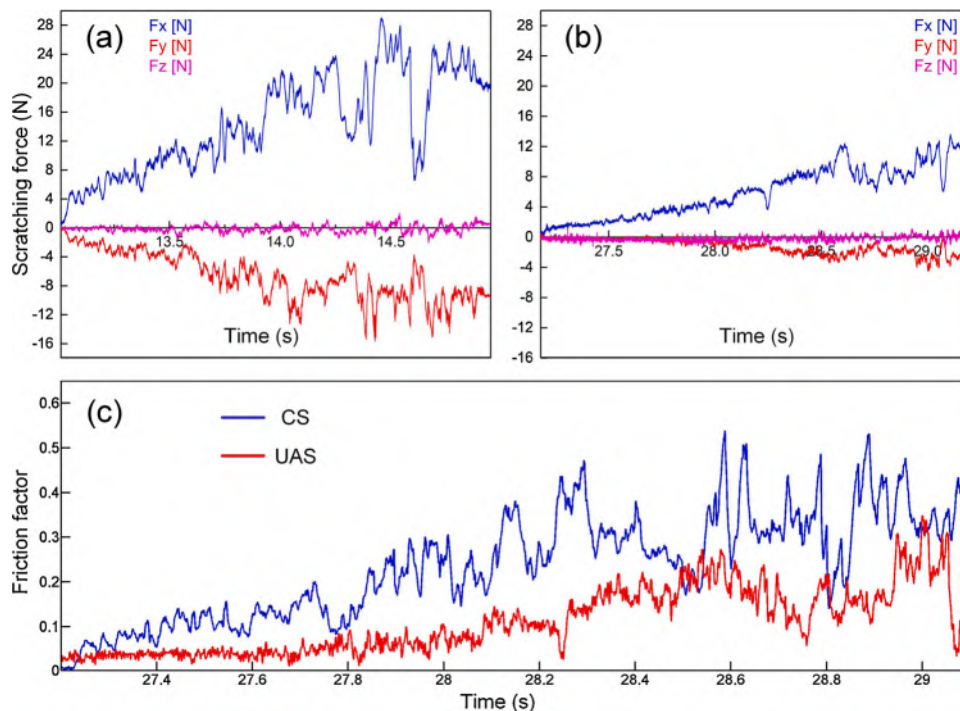

Fig. 12. The variation of scratching force in (a) conventional scratching (CS), (b) continuous scratching assisted by ultrasonic vibration (UAS). (c) The comparison of friction factor.

designed for the intermittent and continuous UAS tests, respectively. The effect of ultrasonic vibration in the intermittent UAS can be distinguished as impact-separation, and the continuous UAS is characterized by reciprocating-polishing.

For the intermittent UAS, the behavior of high frequency impact-separation can increase the critical penetration depth of ductile-brittle transition by over 70 %, and lead to a higher proportion of ductile removal, which helps inhibit the crack initiation of C/SiC during scratching. The minimal volume of material removal by each vibration cycle effectively restrains the fiber rupture as well as random cracking and spalling, thus achieving about 30 % reduction of scratching resistance with less force fluctuation and lower friction factor. However, the high scratching velocity tends to decrease the number of impacts per unit scratching length, and the scratching depth greater than amplitude induces the incomplete separation between indenter and workpiece, which limits the effectiveness of ultrasonic vibration in the surface integrity improvement and force reduction.

For the continuous UAS, the overlapping rate (O_r) and the dynamic shear angle (θ_{max}) are firstly proposed based on the kinematic analysis to evaluate the reciprocating-polishing effect. Larger θ_{max} is benefit to obtain intact fibers by shearing fracture with minimal cracks. And the higher O_r enhances the reciprocating-polishing effect, which helps remove the cracking layer on the scratching grooves, and prevents the clogging of the material debris on the scratching path, leading to a better surface integrity. These interactions contribute to achieve a lower scratching load decreased by about 40 %. While, as the scratching velocity increases, the force reduction rate significantly decreases at low O_r, indicating that the high scratching velocity tends to diminish the effect of ultrasonic vibration in the continuous scratching.

To eliminate the diminishing effect of ultrasonic vibration in different RUM processes, it is proposed that the machining parameters should be matched with vibration frequency and amplitude, for instance, the cutting depth of abrasives should be set comparable to the amplitude to obtain the intermittent cutting characteristics, and proper cutting speed need be adopted to achieve high overlapping rate to enhance the reciprocating-polishing behaviors. These ultrasonic vibration effects are different strategies to change the interactions between the cutting tool and workpiece material to achieve better surface quality and lower cutting force, which is critical in the vibration assisted processing of advanced materials.

CRediT authorship contribution statement

Zhen Li: Methodology, Investigation, Validation, Formal analysis, Writing - original draft. **Songmei Yuan:** Methodology, Supervision, Project administration, Funding acquisition. **Jiang Ma:** Formal analysis, Writing - review & editing, Funding acquisition. **Jun Shen:** Methodology, Supervision, Writing - review & editing. **Andre D.L. Batako:** Conceptualization, Methodology, Writing - review & editing.

Declaration of Competing Interest

The authors declare that they have no known competing financial interests or personal relationships that could have appeared to influence the work reported in this paper.

Acknowledgements

References

Amin, M., Yuan, S.M., Khan, M.Z., Wu, Q., Zhu, G.Y., 2017. Development of a generalized cutting force prediction model for carbon fiber reinforced polymers based on rotary ultrasonic face milling. Int. J. Adv. Manuf. Technol. 93, 2655–2666. https://doi.org/10.1007/s00170-017-0469-9.

Bertsche, E., Ehmann, K., Malukhin, K., 2013. An analytical model of rotary ultrasonic milling. Int. J. Adv. Manuf. Technol. 65, 1705–1720. https://doi.org/10.1007/s00170-012-4292-z.

Brecher, C., Schug, R., Weber, A., Wenzel, C., Hannig, S., 2010. New systematic and time-saving procedure to design cup grinding wheels for the application of ultrasonic-assisted grinding. Int. J. Adv. Manuf. Technol. 47, 153–159. https://doi.org/10.1007/s00170-009-2204-7.

Cao, J.G., Wu, Y.B., Lu, D., Fujimoto, M., Nomura, M., 2014. Material removal behavior in ultrasonic-assisted scratching of SiC ceramics with a single diamond tool. Int. J. Mach. Tools Manuf. 79 (2014), 49–61. https://doi.org/10.1016/j.ijmachtools.2014.02.002.

Diaz, O.G., Axinte, D., 2017. Towards understanding the cutting and fracture mechanism in Ceramic Matrix Composites. Int. J. Mach. Tools Manuf. 118-119, 12–25. https://doi.org/10.1016/j.ijmachtools.2017.03.008.

Diaz, O.G., Luna, G.G., Liao, Z., Axinte, D., 2019. The new challenges of machining Ceramic Matrix Composites (CMCs): review of surface integrity. Int. J. Mach. Tools Manuf. 139, 24–36. https://doi.org/10.1016/j.ijmachtools.2019.01.003.

Ding, K., Fu, Y., Su, H., Chen, Y., Yu, X., Ding, G., 2014. Experimental studies on drilling tool load and machining quality of C/SiC composites in rotary ultrasonic machining. J. Mater. Process. Tech. 214, 2900–2907. https://doi.org/10.1016/j.jmatprotec.2014.06.015.

Feng, P.F., Liang, G.Q., Zhang, J.F., 2014. Ultrasonic vibration-assisted scratch characteristics of silicon carbide-reinforced aluminum matrix composites. Ceram. Int. 40, 10817–10823. https://doi.org/10.1016/j.ceramint.2014.03.073.

Gong, H., Fang, F.Z., Hu, X.T., 2010. Kinematic view of tool life in rotary ultrasonic side milling of hard and brittle materials. Int. J. Mach. Tools Manuf. 50, 303–307. https://doi.org/10.1016/j.ijmachtools.2009.12.006.

Lawn, B.R., Evans, A.G., Marshall, D.B., 1980. Elastic/plastic indentation damage in ceramics: the median/radial crack system. J. Am. Ceram. Soc. 63, 574–581. https://doi.org/10.1111/j.1151-2916.1980.tb10768.x.

Li, Z.C., Jiao, Y., Deines, T.W., Pei, Z.J., Treadwell, C., 2005. Rotary ultrasonic machining of ceramic matrix composites: feasibility study and designed experiments. Int. J. Mach. Tools Manuf. 45, 1402–1411. https://doi.org/10.1016/j.ijmachtools.2005.01.034.

Li, Z., Yuan, S.M., Song, H., Batako, A.D., 2018. A cutting force model based on kinematics analysis for C/SiC in rotary ultrasonic face machining. Int. J. Adv. Manuf. Technol. 97, 1223–1239. https://doi.org/10.1007/s00170-018-1995-9.

Li, Y.C., Ge, X., Wang, H., Hu, Y.B., Ning, F.D., Cong, W.L., Ren, C.Z., 2019. Study of material removal mechanisms in grinding of C/SiC composites via single-abrasive scratch tests. Ceram. Int. 45, 4729–4738. https://doi.org/10.1016/j.ceramint.2018.11.165.

Liang, Z.Q., Wang, X.B., Wu, Y.B., Xie, L.J., Jiao, L., Zhao, W.X., 2013. Experimental study on brittle-ductile transition in elliptical ultrasonic assisted grinding (EUAG) of monocrystal sapphire using single diamond abrasive grain. Int. J. Mach. Tools Manuf. 71, 41–51. https://doi.org/10.1016/j.ijmachtools.2013.04.004.

Liu, D.F., Cong, W.L., Pei, Z.J., Tang, Y.J., 2012. A cutting force model for rotary ultrasonic machining of brittle materials. Int. J. Mach. Tools Manuf. 52, 77–84. https://doi.org/10.1016/j.ijmachtools.2011.09.006.

Lv, D.X., Tang, Y.J., Wang, H.X., Huang, Y.H., 2013. Experimental investigations on subsurface damage in rotary ultrasonic machining of glass BK7. Mach. Sci. Technol. 17, 443–463. https://doi.org/10.1080/10910344.2013.806114.

Msaoubi, R., Axinte, D., Soo, S.L., Nobel, C., Attia, H., Kappmeyer, G., Engin, S., Sim, W. M., 2015. High performance cutting of advanced aerospace alloys and composite materials. CIRP Ann. Manuf. Technol. 64, 557–580. https://doi.org/10.1016/j.cirp.2015.05.002.

Naslain, R., 2004. Design, preparation and properties of non-oxide CMCs for application in engines and nuclear reactors: an overview. Compos. Sci. Technol. 64, 155–170. https://doi.org/10.1016/S0266-3538(03)00230-6.

Ning, F.D., Cong, W.L., Pei, Z.J., Treadwell, C., 2015. Rotary ultrasonic machining of CFRP: a comparison with grinding. Ultrasonics 66, 125–132. https://doi.org/10.1016/j.ultras.2015.11.002.

Orowan, E., 1949. Fracture and strength of solids. Rep. Prog. Phys. 12, 185–232. https://doi.org/10.1088/0034-4885/12/1/309.

Pei, Z.J., Ferreira, P.M., 1999. An experimental investigation of rotary ultrasonic face milling. Int. J. Mach. Tools Manuf. 39, 1327–1344. https://doi.org/10.1016/S0890-6955(98)00093-5.

Pei, Z.J., Ferreira, P.M., Kapoor, S.G., Haselkorn, M., 1995. Rotary ultrasonic machining for face milling of ceramics. Int. J. Mach. Tools Manuf. 35, 1033–1046. https://doi.org/10.1016/0890-6955(94)00100-X.

Teti, R., 2002. Machining of composite materials. CIRP Ann. Manuf. Technol. 51, 611–634. https://doi.org/10.1016/S0007-8506(07)61703-X.

Wang, Y., Lin, B., Zhang, X., 2014. Research on the system matching model in ultrasonic vibration-assisted grinding. Int. J. Adv. Manuf. Technol. 70, 449–458. https://doi.org/10.1007/s00170-013-5269-2.

Wang, Y., Sarin, V.K., Lin, B., Li, H., Gillard, S., 2016. Feasibility study of the ultrasonic vibration filing of carbon fiber reinforced silicon carbide composites. Int. J. Mach. Tools Manuf. 101, 10–17. https://doi.org/10.1016/j.ijmachtools.2015.11.003.

Wang, H., Pei, Z.J., Cong, W.L., 2020. A feeding-directional cutting force model for end surface grinding of CFRP composites using rotary ultrasonic machining with

elliptical ultrasonic vibration. Int. J. Mach. Tools Manuf. 152, 103540 https://doi.org/10.1016/j.ijmachtools.2020.103540.

Yang, X.X., Zhang, B., 2019. Material embrittlement in high strain-rate loading. Int. J. Extr. Manuf. 1, 022003 https://doi.org/10.1088/2631-7990/ab263f.

Yuan, S.M., Fan, H.T., Amin, M., Zhang, C., Guo, M., 2016. A cutting force prediction dynamic model for side milling of ceramic matrix composites C/SiC based on rotary ultrasonic machining. Int. J. Adv. Manuf. Technol. 86, 37–48. https://doi.org/10.1007/s00170-015-8099-6.

Zhang, B., Yin, J.F., 2019. The "skin effect" of subsurface damage distribution in materials subjected to high-speed machining. Int. J. Extr. Manuf. 1, 012007 https://doi.org/10.1088/2631-7990/ab103b.

Zhang, C.L., Feng, P.F., Zhang, J.F., 2013. Ultrasonic vibration-assisted scratch-induced characteristics of C-plane sapphire with a spherical indenter. Int. J. Mach. Tools Manuf. 64, 38–48. https://doi.org/10.1016/j.ijmachtools.2012.07.009.

Zheng, W., Wang, Y.J., Zhou, M., Wang, Q., Ling, L., 2018. Material deformation and removal mechanism of SiCp/Al composites in ultrasonic vibration assisted scratch test. Ceram. Int. 44, 15133–15144. https://doi.org/10.1016/j.ceramint.2018.05.150.

Zhou, M., Zhao, P., 2016. Prediction of critical cutting depth for ductile-brittle transition in ultrasonic vibration assisted grinding of optical glasses. Int. J. Adv. Manuf. Technol. 86, 1775–1784. https://doi.org/10.1007/s00170-015-8274-9.